Waves in Random and Complex Media
Vol. 17, No. 1, February 2007, 55–66

Taylor & Francis
Taylor & Francis

Improved diagonal tensor approximation (DTA) and hybrid DTA/BCGS–FFT method for accurate simulation of 3D inhomogeneous objects in layered media

B. WEI, E. ŞIMŞEK and Q. H. LIU*

Department of Electrical and Computer Engineering, Duke University, Durham, NC, 27708, USA

(Received 4 April 2006; in final form 11 June 2006)

This paper presents an improved diagonal tensor approximation (DTA) and its hybridization with the stabilized biconjugate-gradient fast Fourier transform (BCGS–FFT) algorithm to solve a volume integral equation for three-dimensional (3D) objects in layered media. The improvement in DTA is obtained for lossy media through a higher-order approximation. The interaction between the dyadic Green's function and the contrast source is efficiently evaluated by the (FFT) algorithm through the convolution and correlation theorems. For the hybrid implementation, the DTA solution is used as an initial estimate and a preconditioner in the BCGS–FFT algorithm in order to solve the forwards modelling problem accurately with fewer iterations than the conventional BCGS–FFT algorithm. The accuracy and convergence of the DTA, BCGS–FFT and hybrid DTA/BCGS–FFT methods are compared extensively with several numerical examples. Numerical results show that (a) the improved DTA formulation enhances the accuracy and (b) the DTA/BCGS–FFT method can produce results as accurate as the conventional BCGS–FFT but with fewer iterations if the contrast is moderate. For very high contrasts, the hybrid method does not seem to improve further on the BCGS–FFT iteration convergence.

1. Introduction

Fast and accurate solution of electromagnetic scattering by inhomogeneous three-dimensional (3D) objects of arbitrary shape embedded in a planarly layered medium is one of the most challenging research topics in subsurface sensing because of the complex interactions of waves with the layered background and objects. Such solutions are widely used in subsurface sensing applications such as geophysical exploration, landmine detection and environmental characterization. Direct solution with the finite-element method (FEM) and finite-difference method requires a large number of unknowns because the layered-medium background has to be included in the model. The method of moments (MoM) is a conventional way to solve this scattering problem using the volume electric field integral equation [1,2]. However, MoM is only suitable for small problems owing to its $O(N^2)$ memory usage and $O(N^3)$ central processing unit (CPU) time requirements [or $O(KN^2)$, if an iterative solver is used], where N is the number of the unknowns and K is the number of iterations. To speed up the solution process, several iterative solvers have been developed based on the fast Fourier transform (FFT) algorithm such as the conjugate-gradient (CG) FFT, the biconjugate-gradient (BCG)

*Corresponding author: E-mail: qhliu@ee.duke.edu

Waves in Random and Complex Media
ISSN: 1745-5030 (print), 1745-5049 (online)
http://www.tandf.co.uk/journals
DOI: 10.1080/17455030600924949

FFT, and the stabilized biconjugate-gradient (BCGS) FFT method [3–19]. Even though these methods are more efficient than MoM, they are still not fast enough for very large-scale problems.

Over the past few decades, several approximation techniques have been developed based on either the Born or Rytov approximations. The well-known first-order Born approximation is very efficient for weak scattering and small objects, but is not applicable to high contrasts. Its improved version is the extended Born approximation (EBA), which was originally proposed by Habashy *et al*. [20] and further developed by Torres-Verdin and Habashy [21–23], Yu and Carin [24], Cui *et al*. [9–11], and Liu *et al*. [12–19, 25]. Quasi-linear (QL) and quasi-analytical (QA) approximations are other examples of improved Born approximations [26–29]. Numerical results show that the EBA, QL and QA have better accuracy than the Born approximation; these methods have been successfully applied to forward and inverse problems.

Recently, Song and Liu proposed a novel diagonal tensor approximation (DTA) for 3D objects buried in layered media [30–32], which expresses the scattered fields inside objects as the projection of the background fields via a second-rank scattering tensor (a reflectivity tensor). This scattering tensor is approximated as a source-dependent diagonal tensor based on the principle of superposition. Numerical tests show that this novel approximation has better accuracy and a wider range of applicability than the existing approximations.

In the present work, we first define a new approximation formula for the scattered field to improve the accuracy of DTA by using modified Born series as it is done in [28, 29]. Then, based on the high accuracy and wide range of applicability of DTA and the high efficiency of hybrid methods [13, 14], we combine the DTA with stabilized BCGS–FFT algorithm to form a hybrid DTA/BCGS–FFT algorithm (abbreviated as DTA–BCGS). The inhomogeneous objects are located completely within one single layer in the multilayer medium, so both DTA and BCGS are accelerated by using the FFT algorithm in all directions. For the hybrid implementation, the DTA solution is used as an initial estimate and a preconditioner in the BCGS–FFT algorithm in order to solve the forward modelling problem accurately with fewer iterations than the conventional BCGS–FFT algorithm. The accuracy and convergence of the DTA, BCGS–FFT and hybrid DTA–BCGS are compared extensively. Numerical results show that the modified DTA formulation improves the accuracy with respect to the one proposed in [30]. Moreover, the hybrid DTA–BCGS method can produce results as accurate as the conventional BCGS–FFT but with fewer iterations.

The outline of current paper is as follows: first the brief formulations of integral equations, the modified DTA and its hybridization with BCGS–FFT are presented. Next, several numerical examples are used to verify/compare the accuracy and the efficiency of the new DTA and hybrid DTA–BCGS algorithms with respect to some other approximation or full-wave algorithms. Finally, some discussions and conclusions are given.

2. Formulation

2.1 *Integral equations*

In this work, it is assumed that the measurements are taken on some surface S in layer m and the inhomogeneous objects are contained inside domain D in layer q. The electrical properties of layer q, layer m and the objects are characterized by the complex permittivity $\tilde{\epsilon}_q$, $\tilde{\epsilon}_m$ and $\tilde{\epsilon}$, respectively, which are the combinations of the corresponding material's relative dielectric constant and conductivity. For example, the complex permittivity for an inhomogeneous object is expressed as $\tilde{\epsilon} = \epsilon_0\epsilon_r - j\sigma/\omega$, where ϵ_r is the relative dielectric constant of the object, ϵ_0 the permittivity of free space, σ conductivity of the object, j the imaginary unit and ω

the angular frequency. In the present paper, we assume that the magnetic permeability μ in the target is the same as μ_q in the layered medium, and thus there are no induced magnetic sources. The time dependency of $e^{j\omega t}$ is implied.

The fundamental integral equations are

$$\mathbf{E}_m^{sca}(\mathbf{r}) = j\omega\tilde{\epsilon}_q \int_D \mathbf{G}_{mq}^{EJ}(\mathbf{r}, \mathbf{r}') \cdot \chi(\mathbf{r}')\mathbf{E}(\mathbf{r}')d\mathbf{r}', \quad \mathbf{r} \in S \tag{1}$$

$$\mathbf{E}(\mathbf{r}) = \left(k_q^2 + \nabla\nabla\cdot\right) \int_D \mathbf{G}_{qq}^{AJ}(\mathbf{r}, \mathbf{r}') \cdot \chi(\mathbf{r}')\mathbf{E}(\mathbf{r}')d\mathbf{r}' + \mathbf{E}^{inc}(\mathbf{r}), \quad \mathbf{r} \in D \tag{2}$$

where $\chi(\mathbf{r})$ is the contrast defined as

$$\chi(\mathbf{r}) = \frac{\tilde{\epsilon}(\mathbf{r})}{\tilde{\epsilon}_q} - 1 \tag{3}$$

and $\mathbf{G}_{mq}^{EJ}(\mathbf{r}, \mathbf{r}')$ is the electric dyadic Green's function at the field point $\mathbf{r}$ in layer m related to a unit current source at the point $\mathbf{r}'$ in layer q, $\mathbf{G}_{qq}^{AJ}(\mathbf{r}, \mathbf{r}')$ is an auxiliary dyadic Green's function representing the magnetic vector potential, and the wavenumber in layer q is given by $k_q^2 = \omega^2\mu_q\tilde{\epsilon}_q$. Equation (1) is called the 'data equation,' which defines the scattered field at the observation point. Equation (2) is called the 'object equation,' which is the Fredholm integral equation of the second kind for the unknown field inside the object. Note that when the total electric field inside D is obtained, the observed scattered field can be calculated by equation (1). However, here we are trying to find out a simplified form representing the total electric field within D instead of solving equation (2) directly.

The evaluation of the layered-medium Green's functions is one of the most important and time-consuming ingredients of the integral equations [10, 33]. Here, we have developed a recursive matrix method to calculate the Green's functions efficiently. In this method, we define three coefficient matrices, whose elements are some basic Sommerfeld integrals, in such a way that any Green's function component can be expressed as a combination of these elements. The recursive calculation of coefficient matrices by using the boundary conditions at the layers interfaces makes it possible to calculate the Green's functions, simply by changing the positions of the source terms in the matrix equations. Note that, in equation (2) $\mathbf{G}^{AJ}$ is used instead of $\mathbf{G}^{EJ}$ in order to avoid singularity, as it is done in [4] for free space and [16, 18, 19] for layered media. Furthermore, the calculation of Green's functions has been accelerated by singularity subtraction [33].

2.2 *The diagonal tensor approximation (DTA)*

The total electric field at $\mathbf{r}$ created by an exciting source located at $\mathbf{r}_T$ can be written as a summation of the incident and scattered fields based on the superposition principle [34] as follows

$$\mathbf{E}(\mathbf{r}, \mathbf{r}_T) = \mathbf{E}^{inc}(\mathbf{r}, \mathbf{r}_T) + \mathbf{E}^{sca}(\mathbf{r}, \mathbf{r}_T). \tag{4}$$

The scattered field can be approximately related to the incident field by a source-dependent scattering tensor $\Gamma(\mathbf{r}, \mathbf{r}_T)$, i.e.

$$\mathbf{E}^{sca}(\mathbf{r}, \mathbf{r}_T) \approx \Gamma(\mathbf{r}, \mathbf{r}_T) \cdot \mathbf{E}^{inc}(\mathbf{r}, \mathbf{r}_T). \quad \mathbf{r} \in D. \tag{5}$$

Then the total field can be written as

$$\mathbf{E}(\mathbf{r}, \mathbf{r}_T) \approx [\mathbf{I} + \Gamma(\mathbf{r}, \mathbf{r}_T)] \cdot \mathbf{E}^{inc}(\mathbf{r}, \mathbf{r}_T). \quad \mathbf{r} \in D, \tag{6}$$

where $\mathbf{I}$ is an identity matrix. When the cross-polarization is weak, it can be assumed that each component of the scattered field or the total field is only related to the corresponding component of the incident field. According to this assumption, the scattering tensor can be approximated by the following diagonal form

$$\Gamma \approx \begin{bmatrix} \gamma_x & 0 & 0 \\ 0 & \gamma_y & 0 \\ 0 & 0 & \gamma_z \end{bmatrix}. \tag{7}$$

This approximation is called DTA. For the analytical expressions of the unknown components of the diagonal scattering tensor, the localized nonlinear approximation is used, similar to [20]. The details of this procedure and some important discussions can be found in [30] and [31]. Simply, the scattered field in equation (2) can be approximated by using the DTA as follows,

$$\begin{aligned} \mathbf{E}^{sca}(\mathbf{r}, \mathbf{r}_T) = \left(k_q^2 + \nabla\nabla\cdot\right) \int_D \mathbf{G}_{qq}^{AJ}(\mathbf{r}, \mathbf{r}') \cdot \chi(\mathbf{r}') \\ \cdot[\mathbf{I} + \Gamma(\mathbf{r}', \mathbf{r}_T)] \cdot \mathbf{E}^{inc}(\mathbf{r}', \mathbf{r}_T) d\mathbf{r}'. \quad \mathbf{r} \in D. \end{aligned} \tag{8}$$

Numerically it is shown that DTA has better accuracy than the existing approximations such as EBA for the same electric contrast while its computational speed is essentially the same [30, 31]. In [28] and [35–37], it is shown that the modified Born series or modified Neumann series has better convergence than Born series for lossy media. In this work, to improve the accuracy of the DTA by constructing higher-order DTA in a manner similar to the QA and QL series for QA and QL approximations in [28] and [29], respectively, we define a new approximation formula for the scattered field as follows

$$\begin{aligned} \mathbf{E}^{sca}(\mathbf{r}, \mathbf{r}_T) = \alpha\left(k_q^2 + \nabla\nabla\cdot\right) \int_D \mathbf{G}_{qq}^{AJ}(\mathbf{r}, \mathbf{r}') \cdot \chi(\mathbf{r}') \\ [\mathbf{I} + \Gamma(\mathbf{r}', \mathbf{r}_T)] \cdot \mathbf{E}^{inc}(\mathbf{r}', \mathbf{r}_T) d\mathbf{r}' \\ + (1 - \alpha)\, \Gamma(\mathbf{r}, \mathbf{r}_T) \cdot \mathbf{E}^{inc} \end{aligned} \tag{9}$$

where

$$\alpha = \frac{2\sigma_q}{(\sigma + \sigma_q) + j\omega(\epsilon - \epsilon_q)}. \tag{10}$$

Note that outside the object domain D, $\alpha = 1$, equation (9) reduces to equation (8) as the contrast is zero there. From the mathematical point of view, equation (8) and equation (9) can be seen as zeroth-order and first-order DTA approximations, respectively, and as it has been done in [28], the higher orders can be obtained. In the present work, we only consider the first-order approximation that improves the accuracy in lossy media with respect to the zeroth-order approximation as it has been shown in [28].

2.3 *The hybridization of DTA with BCGS–FFT algorithm for integral equations*

Equation (2) can be written compactly as

$$\mathcal{L}[\tilde{\mathbf{D}}(\mathbf{r})] = \mathbf{E}^{inc}(\mathbf{r}), \quad \mathbf{r} \in D \tag{11}$$

where $\tilde{\mathbf{D}}(\mathbf{r}) = \tilde{\epsilon}(\mathbf{r})\mathbf{E}(\mathbf{r})/\epsilon_q$, and $\mathcal{L}$ is a linear operator defined as

$$\mathcal{L}[\,] = \frac{\epsilon_q[\,]}{\tilde{\epsilon}(\mathbf{r})} - \left(k_q^2 + \nabla\nabla\cdot\right) \int_D \mathbf{G}_{qq}^{AJ}(\mathbf{r}, \mathbf{r}') \cdot \tilde{\chi}(\mathbf{r}')[\,] d\mathbf{r}' \tag{12}$$

where the contrast $\tilde{\chi}(\mathbf{r})$ is defined as

$$\tilde{\chi}(\mathbf{r}) = \frac{\tilde{\epsilon}(\mathbf{r}) - \tilde{\epsilon}_q}{\tilde{\epsilon}(\mathbf{r})}. \tag{13}$$

The discrete form of equation (11) can be obtained by using Galerkin's method. In this work, both basis and testing functions are "roof-top" functions [4, 12]. The resulting discrete linear system can be written as

$$\tilde{\mathcal{L}}[\mathbf{d}] = \mathbf{e}^{inc} \tag{14}$$

where $\mathbf{d}$ and $\mathbf{e}^{inc}$ are vectors of the unknown electric flux density and incident electric field, respectively, which are defined at the centre of each cell surface. Equation (14) can be solved iteratively using the BCGS method, and the FFT technique is applied during each iteration. The details of this procedure can be found in [15] and [16]. To reduce the number of iterations used in the BCGS–FFT method, the solution obtained from DTA can be used as an initial estimate and/or a preconditioner for the BCGS–FFT, which forms the hybrid DTA/BCGS–FFT method, or simply DTA–BCGS. The algorithm of this method can be explained as follows.

Assume that $\mathbf{E}^{DTA}$ is the approximation of the solution obtained with DTA and $\tilde{\mathbf{D}}^{DTA} = \tilde{\epsilon}(\mathbf{r})\mathbf{E}^{DTA}/\epsilon_q$. By using the linear operator defined in (12), both equations, (8) and (9) can be written as

$$\mathcal{L}_{DTA}^{-1}[\mathbf{E}^{inc}(\mathbf{r})] = \tilde{\mathbf{D}}^{DTA}(\mathbf{r}), \qquad \mathbf{r} \in D \tag{15}$$

and after discretization equation (15) becomes

$$\tilde{\mathcal{L}}_{DTA}^{-1}[\mathbf{e}^{inc}] = \mathbf{d}^{DTA}, \tag{16}$$

where $\tilde{\mathcal{L}}_{DTA}^{-1}$ is the DTA linear operator, and $\mathbf{d}^{DTA}$ is a vector representing the electric flux density under the approximation of DTA. By combining equations (14) and (16), we obtain the following equivalent linear system

$$\tilde{\mathcal{L}}_{DTA}^{-1}\tilde{\mathcal{L}}[\mathbf{d}] = \mathbf{d}^{DTA}.$$

To solve equation (17), DTA solution is used an initial estimate, i.e. $\mathbf{d}_0 = \mathbf{d}^{DTA}$, and then residuals are computed as follows

$$\mathbf{r}_0 = \mathbf{d}^{DTA} - \tilde{\mathcal{L}}_{DTA}^{-1}\tilde{\mathcal{L}}[\mathbf{d}_0], \quad \rho_0 = \varrho = \omega_0 = 1, \quad \mathbf{v}_0 = \mathbf{p}_0 = 0.$$

With the choice of an arbitrary vector $\tilde{\mathbf{r}}_0$ such that $(\tilde{\mathbf{r}}_0, \mathbf{r}_0) \neq 0$, e.g., $\tilde{\mathbf{r}}_0 = \mathbf{r}_0$ or $\tilde{\mathbf{r}}_0 = \mathbf{d}^{DTA}$, in the ith iteration, we compute

$$\rho_i = (\tilde{\mathbf{r}}_0, \mathbf{r}_{i-1}), \quad \beta = \varrho\rho_i/(\omega_{i-1}\rho_{i-1}), \quad \mathbf{p}_i = \mathbf{r}_{i-1} + \beta(\mathbf{p}_{i-1} - \omega_{i-1}\mathbf{v}_{i-1}),$$
$$\mathbf{y} = \tilde{\mathcal{L}}\mathbf{p}_i, \quad \mathbf{v}_i = \tilde{\mathcal{L}}_{DTA}^{-1}\mathbf{y}, \quad \varrho = \rho_i/(\tilde{\mathbf{r}}_0, \mathbf{v}_i), \quad \mathbf{s} = \mathbf{r}_{i-1} - \varrho\mathbf{v}_i, \quad \mathbf{y} = \tilde{L}\mathbf{s},$$
$$\mathbf{t} = \tilde{\mathcal{L}}_{DTA}^{-1}\mathbf{y}, \quad \omega_i = (\mathbf{t}, \mathbf{s})/(\mathbf{t}, \mathbf{t}), \quad \mathbf{d}_i = \mathbf{d}_{i-1} + \varrho\mathbf{p}_i + \omega_i\mathbf{s}, \quad \mathbf{r}_i = \mathbf{s} - \omega_i\mathbf{t}.$$

The iterative solver is ended when $\|\mathbf{s}\|/\|\mathbf{d}^{DTA}\|$ or $\|\mathbf{r}_i\|/\|\mathbf{d}^{DTA}\|$ becomes smaller than the given error criterion.

3. Discussions

The preconditioner, $\tilde{\mathcal{L}}_{DTA}^{-1}$, can be obtained efficiently by using the FFT algorithm and equation (17) can be solved efficiently by the BCGS–FFT method. By using the DTA result as an initial estimate and a preconditioner, this hybrid DTA–BCGS algorithm converges much faster than the regular BCGS–FFT method if the contrast is moderate. It can be shown

Table 1. Abbreviations.

Abbreviation	Method
DTA1	DTA by using equation (8).
DTA2	DTA by using equation (9).
DTA2–BCGS	Hybrid DTA–BCGS method by using the DTA2 result as an initial estimate and a preconditioner.
BCGSini	Hybrid DTA–BCGS method by using the DTA2 result as an initial estimate.

from equation (17) that for low electric contrasts, $\mathbf{d}^{DTA}$ is very close to $\mathbf{d}$ and hence the operator $\tilde{\mathcal{L}}_{DTA}^{-1}\tilde{\mathcal{L}}$ is very close to the identity matrix. However, the increase of the electric contrast decreases the accuracy of DTA and the preconditioning loses its efficiency. In the following examples only moderate contrast problems with high accuracy requirement are considered.

4. Numerical examples

To verify the improvement in diagonal tensor approximation, and the efficiency/accuracy of the hybrid method, four different methods have been used in addition to the regular BCGS–FFT solution. These methods and the abbreviations used for them are given in table 1.

For the following examples, the permeability of the background and the objects are assumed to be μ_0.

4.1 *Experiment Set-ups*

There are six different experiment set-ups: first three examples are chosen to illustrate the microwave detection problems with a high-operating frequency (HF), and in the last three examples low-operating frequencies (LF) are used to illustrate the induction problems. The experiment set-ups are described below.

Set-up 1: A homogeneous cuboid in a three-layer medium, HF

A homogeneous cuboid with the dimensions of $a = 1.6$ m, $b = 1.6$ m and $c = 1.15$ m is located at the bottom layer of a three-layer background, shown as figure 1(a). The center of the cuboid is at (2.05, −2.05, 1.425) m. The interface positions are at $z_0 = 0.0$ m and $z_1 = 0.5$ m, the distance between z_1 and the top of the cuboid is $d = 0.35$ m. The electrical parameters of the background are: $\epsilon_{r0} = 1.0, \sigma_0 = 0.0$ S/m; $\epsilon_{r1} = 1.5, \sigma_1 = 0.002$ S/m; $\epsilon_{r2} = 2.0, \sigma_2 = 0.01$ S/m. The electrical parameters of the cuboid are $\epsilon_r = 8.0$ and $\sigma = 0.02$ S/m. A vertical unit electric dipole located at (2.05, −2.05, −0.425) m is used as a source with 10 MHz operating frequency.

Set-up 2: A homogeneous cylinder in a five-layer medium, HF

In this example, a homogeneous cylinder, with the radius of 0.8 m and height of 1.15 m, is located in the middle layer of a five-layer background, shown as figure 1(b). The center of the cylinder is located at (2.05, −2.05, 1.425) m; $z_0 = 0.0$ m, $z_1 = 0.5$ m, $z_2 = 2.35$ m, and $z_3 = 2.85$ m, the distance between z_1 and the top of the cylinder is $d = 0.35$ m. The electrical parameters of the background are: $\epsilon_{r0} = 1.0$, $\sigma_0 = 0.0$ S/m; $\epsilon_{r1} = 1.21$, $\sigma_1 = 0.01$ S/m; $\epsilon_{r2} = 6.0$, $\sigma_2 = 0.03$ S/m; $\epsilon_{r3} = 1.21$, $\sigma_3 = 0.01$ S/m; $\epsilon_{r4} = 1.0$, $\sigma_4 = 0.0$ S/m. The electrical parameters of the cylinder are $\epsilon_r = 2.0, \sigma = 0.015$ S/m. The location of the vertical electric dipole is (2.05, −2.05, −0.425) m. The operating frequency is 100 MHz.

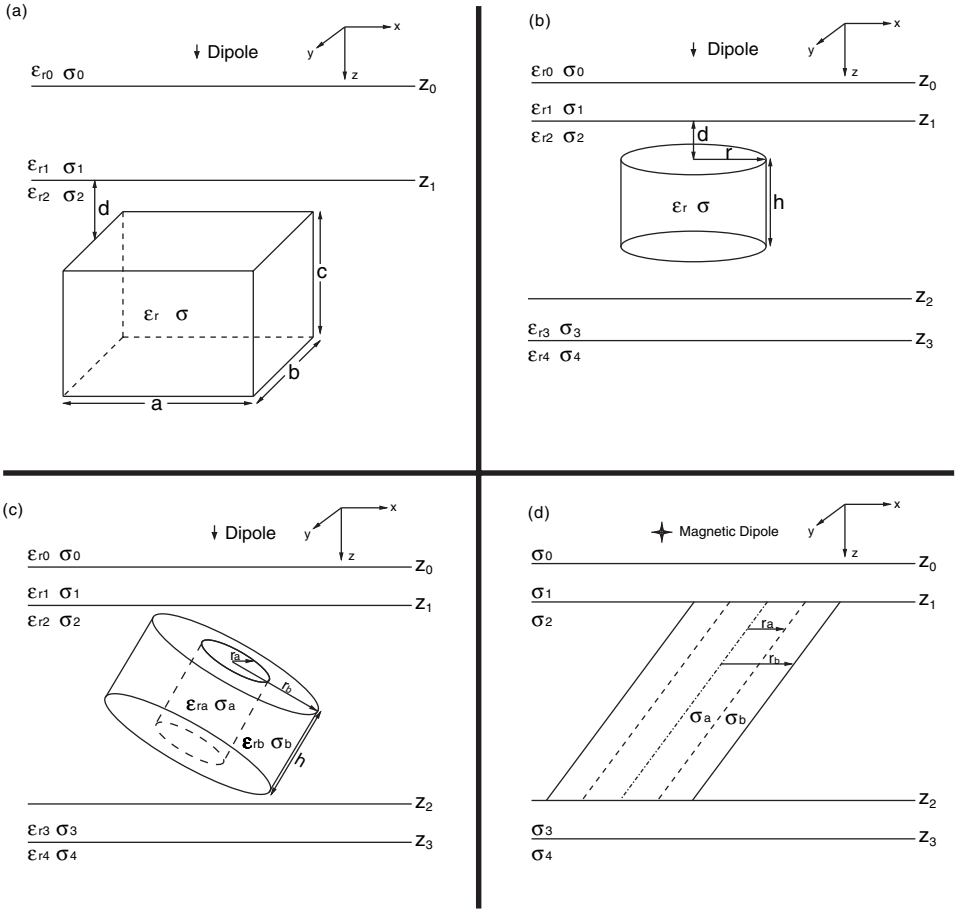

Figure 1. (a) A homogeneous cuboid in a three-layer medium. (b) A homogeneous cylinder in a five-layer medium. (c) A two-layer tilted cylinder in a five-layer background. (d) A two-layer deformed cylinder in a five-layer medium.

Set-up 3: A two-layer tilted cylinder in a five-layer medium, HF

Figure 1(c) shows a two-layer tilted cylinder with the height of 1.0 m which is centered at (2.05, −2.05, 1.75) m in a five-layer background. $z_0 = 0.0$ m, $z_1 = 0.5$ m, $z_2 = 3.0$ m and $z_3 = 3.5$ m. The electrical parameters of the background are: $\epsilon_{r0} = 1.0$, $\sigma_0 = 0.0$ S/m; $\epsilon_{r1} = 1.21$, $\sigma_1 = 0.01$ S/m; $\epsilon_{r2} = 2.0$, $\sigma_2 = 0.05$ S/m; $\epsilon_{r3} = 1.21$, $\sigma_3 = 0.1$ S/m; $\epsilon_{r4} = 1.0$, $\sigma_4 = 0.0$ S/m. The cylinder is tilted with 30° angle on the x–z plane. The radius and electrical parameters of the inner cylinder are $r_a = 0.4$ m, $\epsilon_{ra} = 8.0$, $\sigma_a = 0.15$ S/m. The radius and electrical parameters of the outer cylinder are $r_b = 0.8$ m, $\epsilon_{rb} = 4.0$, $\sigma_b = 0.08$ S/m. The location of the electric dipole is (2.05, −2.05, −0.425) m, in the top layer. The operating frequency is $f = 100$ MHz.

Set-up 4: A homogeneous cuboid in a three-layer medium, LF

For the simulation of the detection problems within the induction domain, a unit magnetic dipole is located at (2.15, −2.05, −0.425) m in a three-layer medium, which contains a homogeneous cuboid, as shown in figure 1(a). All the physical quantities are the same as set-up 1, except the ones mentioned here. The conductivities of the layers are: $\sigma_0 = 0.8$ S/m; $\sigma_1 = 0.05$ S/m; $\sigma_2 = 1.0$ S/m. The conductivity of the cuboid is $\sigma = 0.33$ S/m. The frequency is 20 kHz. Since the frequency is low, the influence of the dielectric constant can be neglected.

Set-up 5: A homogeneous cylinder in a five-layer medium, LF

A unit vertical magnetic dipole, operating at $f = 20$ kHz, is located at (2.1, −2.1, −0.425) m in a five-layer medium, which contains a homogeneous cylinder, as shown in figure 1(b). All the physical quantities are the same as set-up 2, except the ones mentioned here. The conductivities of the background are: $\sigma_0 = 0.04$ S/m; $\sigma_1 = 1.0$ S/m; $\sigma_2 = 0.5$ S/m; $\sigma_3 = 1.0$ S/m; $\sigma_4 = 0.05$ S/m. The conductivity of the cylinder is $\sigma = 1.0$ S/m.

Set-up 6: A two-layer deformed cylinder in a five-layer medium

A two-layer deformed cylinder with the height of 2.3 m is centred at (2.05, −2.05, 1.75) m in a five-layer medium, depicted in figure 1(d). The cylinder is tilted with 30° angle on the x–z plane. The radius and conductivity of the inner cylinder are $r_a = 0.2$ m, $\sigma_a = 0.4$ S/m. The radius and conductivity of the outer cylinder are $r_b = 0.4$ m, $\sigma_b = 1.2$ S/m. $z_0 = 0.0$ m, $z_1 = 0.5$ m, $z_2 = 3.0$ m and $z_3 = 3.5$ m. The conductivities of the background are: $\sigma_0 = 0.8$ S/m; $\sigma_1 = 0.04$ S/m; $\sigma_2 = 1.0$ S/m; $\sigma_3 = 0.08$ S/m; $\sigma_4 = 0.6$ S/m. The location of x directed the magnetic dipole is $r_T = (2.05, -2.05, -0.425)$ m in the top layer and the frequency is 20 kHz.

4.2 *DTA versus improved DTA*

Figures 2(a–f) show the magnitudes of E_z or E_y obtained with four different methods (DTA1, DTA2, DTA2-BCGS, and BCGS-FFT) for set up 1–6, respectively. Figure 2(f) also shows the incident electric field along the line centering the deformed cylinders for set-up-6 in the absence of the cylinders. For low frequency examples ($f = 20$ kHz), see set-up 4–6 for the details, DTA1 results are very close to the full-wave solutions; but when we look at the DTA2 results, they are almost same as the full-wave solutions, figures 2(d–f). When we increase the frequency ($f = 10$ MHz for set up 1, $f = 100$ MHz for set-up 2 and 3), the difference between DTA1 and BCGS-FFT solutions increases. This is also true for DTA2 solutions; however DTA2 results are more accurate than DTA1 results. These numerical experiments clearly demonstrate that the modification in the diagonal tensor improves the accuracy of the approximation.

Another observation is that the results obtained by using the DTA2 result as an initial estimate and a preconditioner, shown as DTA2-BCGS, are the same as the BCGS–FFT results, as expected.

Note that E_z is discontinuous across the interface of the tilted cylinder for set-up 3.

4.3 *Efficiency of the hybrid DTA-BCGS algorithm*

In the previous part, we show that the improved DTA is more accurate than the previous DTA implementation. Here, we demonstrate the efficiency of the hybrid DTA–BCGS algorithm, which uses the DTA2 result as an initial estimate and a preconditioner. For comparison purpose, we also show the results using DTA as the initial solution of BCGS-FFT, which is denoted as BCGSini in the figures.

Figures 3(a–f) shows the residual errors in the BCGS–FFT, BCGSini and DTA–BCGS algorithms as a function of iteration number for set-ups 1–6, respectively. In all examples, it is clear that the DTA–BCGS is the most efficient algorithm with respect to the other algorithms. The number of iterations used for DTA–BCGS is almost half of the ones used for BCGS–FFT in order to obtain the desired accuracy level. Using DTA result as an initial estimate helps to decrease the iteration number but it is not as effective as the preconditioning. This examples show clearly the efficiency and the necessity of the preconditioning.

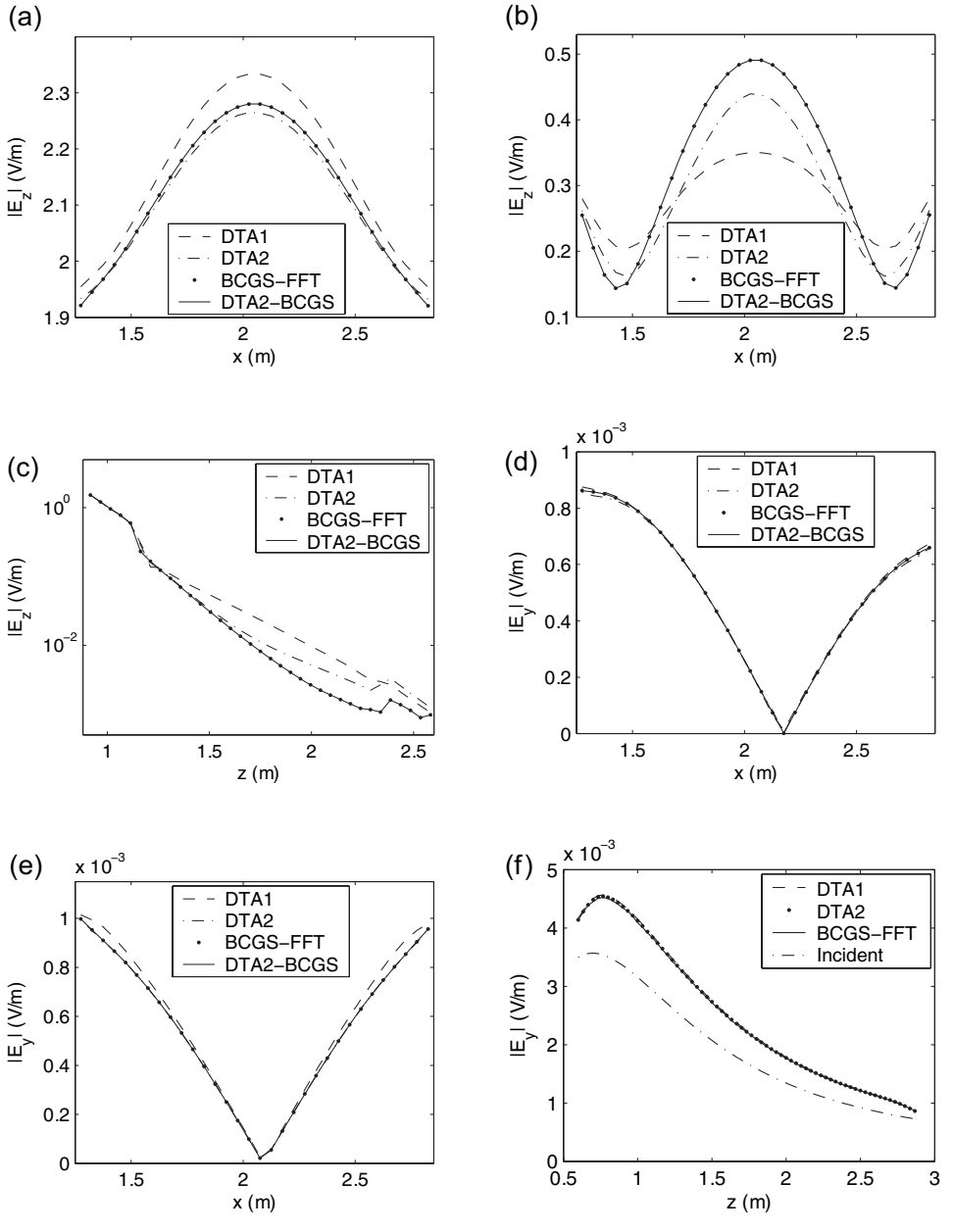

Figure 2. The magnitude of E_z or E_y obtained with four different methods (DTA1, DTA2, DTA2-BCGS and BCGS–FFT). (a) $|E_z|$ as a function of x at $y = -2.05$ m and $z = 1.85$ m for set-up 1. (b) $|E_z|$ as a function of x at $y = -2.05$ m and $z = 1.85$ m for set-up 2. (c) $|E_z|$ as a function of z at $x = 2.0$ m and $y = -2.05$ m for set-up 3. (d) $|E_y|$ as a function of x at $y = -2.05$ m and $z = 1.6$ m for set-up 4. (e) $|E_y|$ as a function of x at $y = -2.05$ m and $z = 1.6$ m for set-up 5. (f) $|E_y|$ as a function of z along the line centering the deformed cylinders for set-up 6.

In all examples, the first residual error of DTA–BCGS or BCGSini solution is smaller than the first residual error of BCGS–FFT solution which also shows that DTA is more accurate than the Born approximation.

Note that figure 3(f) shows the residual errors in BCGS–FFT and BCGSini only, as a function of iteration number. For this example, even using DTA1 result as an initial estimate

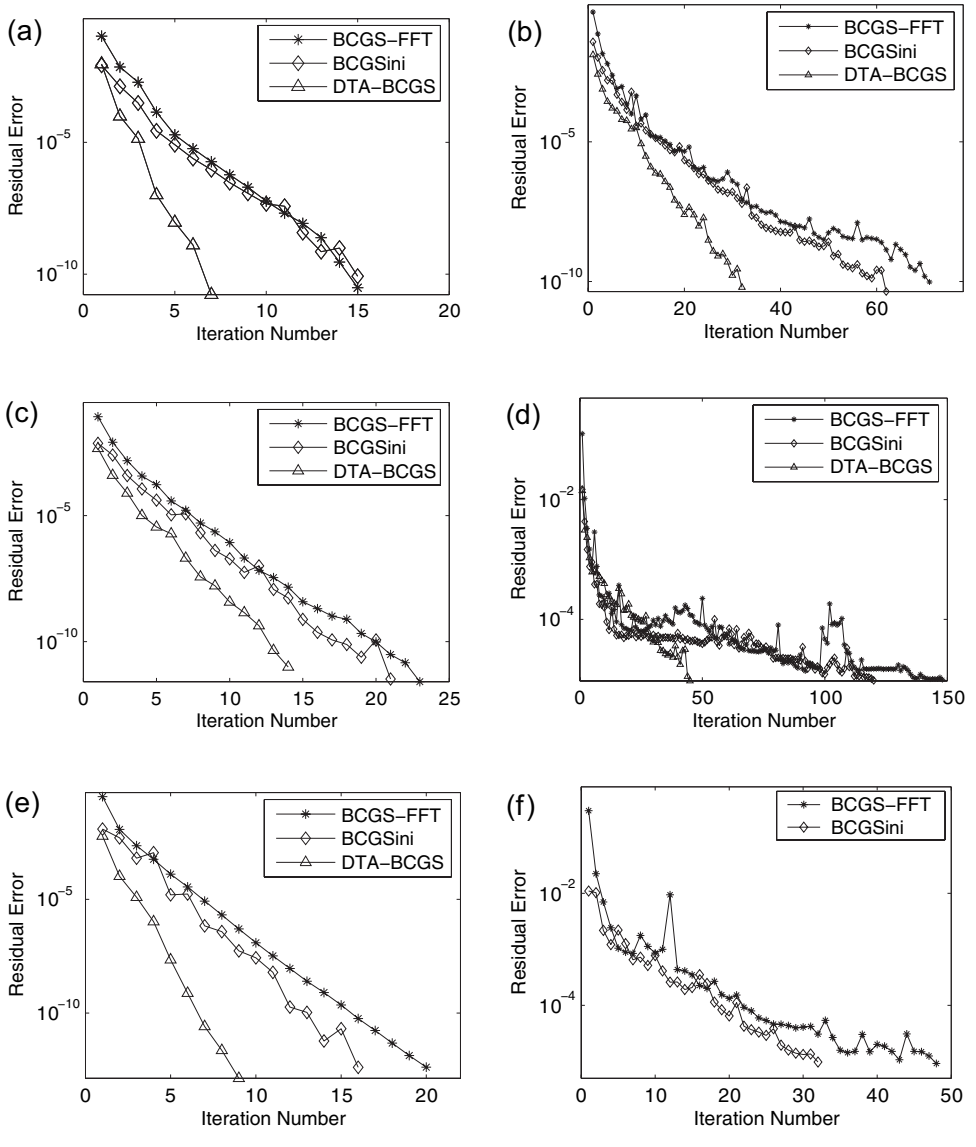

Figure 3. Residual errors in the BCGS-FFT, BCGSini and DTA-BCGS algorithms as a function of iteration number for set-up 1–6.

for BCGS-FFT algorithm helps to reduce the iteration number to meet the required error tolerance. Very similar results to the ones presented here have been obtained for a z-directed magnetic dipole; they are not shown here for brevity.

5. Conclusion

First, the formulation of an improved diagonal tensor approximation is presented and its accuracy was compared with the original DTA proposed by Song and Liu in [30]. Numerical results show that the improved DTA is more accurate than the original DTA. Second, we develop a hybrid DTA–BCGS algorithm for the volume integral equation to improve the accuracy

and efficiency of the simulation of 3D electromagnetic scattering problems in layered media. For the hybrid implementation, DTA is combined with the BCGS–FFT algorithm by using its solution as an initial estimate and as a preconditioner for the BCGS–FFT algorithm. It is shown that the hybrid DTA–BCGS method can produce results as accurate as the conventional BCGS–FFT but requires fewer iterations than the BCGS–FFT method. As a result, the new DTA has better accuracy and wider range of applicability than the original DTA, and its hybridization with BCGS–FFT has better convergence with respect to the conventional BCGS–FFT.

References

[1] Wannamaker, P. E., Hohmann, G. W. and San Filipo, W. A., 1984, Electromagnetic modeling of three-dimensional bodies in layered earths using integral equations. *Geophysics*, **49**, 60–74.

[2] Cui, T. J., Wiesbeck, W. and Herschlein, A., 1998, Electromagnetic scattering by multiple dielectric and conducting objects buried under multi-layered media. Part I: Theory. Part II: Numerical implementation and results. *IEEE Transactions on Geoscience and Remote Sensing*, **36**, 526–546.

[3] Catedra, M. F., Gago, E. and Nuno, L., 1989, A numerical scheme to obtain the RCS of three-dimensional bodies of resonant size using the conjugate gradient method and the fast Fourier transform. *IEEE Transactions on Antennas and Propagation*, **37**, 528–537.

[4] Zwamborn, P. and van den Berg, P. M., 1992, The three dimensional weak form of the conjugate gradient FFT method for solving scattering problems. *IEEE Transactions on Microwave Theory and Technology*, **9**, 1757–1766.

[5] Su, C. C., 1993, The three-dimensional algorithm of solving the electric field integral equation using face-centered node points, conjugate gradient method, and FFT. *IEEE Transactions on Microwave Theory and Technology*, **41**, 510–515.

[6] Gan, H. and Chew, W. C., 1995, A discrete BCG-FFT algorithm for solving 3D inhomogeneous scatter problems. *Journal of Electromagnetic Waves Application*, **9**, 1339–1357.

[7] Cui, T. J. and Chew, W. C., 1999, Fast algorithm for electromagnetic scattering by buried 3D dielectric objects of large size. *IEEE Transactions on Geoscience Remote Sensing*, **37**, 2597–2608.

[8] Cui, T. J. and Chew, W. C., 2000, Novel diffraction tomographic algorithm for imaging two-dimensional dielectric objects buried under a lossy earth. *IEEE Transactions on Geoscience and Remote Sensing*, **38**, 2033–2041.

[9] Cui, T. J., Chew, W. C., Aydiner, A. A. and Chen, S. Y., 2001, Inverse scattering of 2D dielectric objects buried in a lossy earth using the distorted Born iterative method. *IEEE Transactions on Geoscience and Remote Sensing*, **39**, 339–346.

[10] Cui, T. J., Chew, W. C., Aydiner, A. A. and Zhang, Y. H., 2003, Fast-forward solvers for the low-frequency detection of buried dielectric objects. *IEEE Transactions on Geoscience and Remote Sensing*, **41**, 2026–2036.

[11] Cui, T. J., Chew, W. C. and Hong, W., 2004, New approximate formulations for EM scattering by dielectric objects. *IEEE Transactions on Antennas and Propagation*, **52**, 684–692.

[12] Zhang, Z. Q. and Liu, Q. H., 2001, Three-dimensional weak-form conjugate and biconjugate-gradient FFT methods for volume integral equations. *Microwave and Optical Technology Letters*, **29**, 350–356.

[13] Zhang, Z. Q. and Liu, Q. H., 2001, The hybrid extended Born approximation and CG-FFHT method for axisymmetric media. *IEEE Transactions on Geoscience and Remote Sensing*, **39**, 710–717.

[14] Liu, Q. H., Zhang, Z. Q. and Xu, X. M., 2001, The hybrid extended Born approximation and CG-FFT method for electromagnetic induction problems. *IEEE Transactions on Geoscience and Remote Sensing*, **39**, 347–355.

[15] Xu, X. M., Liu, Q. H. and Zhang, Z. Q., 2002, The stabilized biconjugate gradient fast Fourier transform method for electromagnetic scattering. *Journal of Applied Computer Electromagnetic. Society*, **17-1**, 97–103.

[16] Xu, X. M. and Liu, Q. H., 2002, The BCGS-FFT method for electromagnetic scattering from inhomogeneous objects in a layered medium. *IEEE Transactions on Antennas Wireless Propagation Letters*, **1**, 77–80.

[17] Zhang, Z. Q., Liu, Q. H. and Xu, X. M., 2003, RCS computation of large inhomogeneous objects using a fast integral equation solver. *IEEE Transactions on Antennas and Propagation*, **51**, 613-618.

[18] Millard, X. and Liu, Q. H., 2003, A fast volume integral equation solver for electromagnetic scattering from large inhomogeneous objects in layered media. *IEEE Transactions on Antennas and Propagation*, **51**, 2393–2401.

[19] Millard, X. and Liu, Q. H., 2004, Simulation of near-surface detection of objects in layered media by the BCGS-FFT method. *IEEE Transactions on Geoscience of and Remote Sensing*, **42**, 327–334.

[20] Li, F., Liu, Q. H. and Song, L. P., 2004, Three-dimensional reconstruction of objects buried in layered media using Born and distorted Born iterative methods. *IEEE Transactions on Geoscience and Remote Sensing Lett*, **1**, 107–111.

[21] Habashy, T. M., Groom, R. W. and Spies, B. R., 1993, Beyond the Born and Rytov approximations: a nonlinear approach to electromagnetic scattering. *Journal of Geophysical Research*, **98(B2)**, 1759–1775.

[22] Torres-Verdin, C. and Habashy, T. M., 1994, Rapid 2.5-dimensional forward modeling and inversion via a new nonlinear scattering approximation. *Radio Science*, **29**, 1051–1079.

[23] Torres-Verdin, C. and Habashy, T. M., 1995, A two-step linear inversion of two-dimensional conductivity. *IEEE Transactions on Antennas and Propagation*, **43**, 405–415.
[24] Torres-Verdin, C. and Habashy, T. M., 2001, Rapid numerical simulation of axisymmetric single-well induction data using the extended Born approximation. *Radio Science*, **36**, 1287–1306.
[25] Yu, T. J. and Carin, L., 2000, Analysis of the electromagnetic inductive response of a void in a conducting-soil background. *IEEE Transactions on Geoscience and Remote Sensing*, **38**, 1320–1327.
[26] Zhdanov, M. S. and Fang, S., 1996, Three-dimensional quasi-linear electromagnetic inversion. *Radio Science*, **31**, 741–754.
[27] Zhdanov, M. S. and Fang, S., 1996, Quasi-linear approximation in 3D electromagnetic modeling. *Geophysics*, **61**, 646–665.
[28] Zhdanov, M. S. and Fang, S., 1997, Quasi-linear series in three-dimensional electromagnetic modeling. *Radio Science*, **32**, 2167–2188.
[29] Zhdanov, M. S., Dmitriev, V. I., Fang, S. and Hursan, G., 2000, Quasi-analytical approximations and series in electromagnetic modeling. *Geophysics*, **65**, 1746–1757.
[30] Song, L. P. and Liu, Q. H., 2004, Fast three-dimensional electromagnetic nonlinear inversion in layered media with a novel scattering approximation. *Inverse Problems*, **20**, S171–S194.
[31] Song, L. P. and Liu, Q. H., 2005, A new approximation to three dimensional electromagnetic scattering. *IEEE Transactions on Geoscience and Remote Sensing Letters*, **2**, 238–242.
[32] Yu, C., Song, L. P. and Liu, Q. H., 2005, Inversion of multi-frequency experimental data for imaging complex objects by a DTA-CSI method. *Inverse Problems*, **21**, S165–S178.
[33] Simsek, E., Liu, Q. H. and Wei, B., 2006, Singularity subtraction for evaluation of Green's functions for multilayer media. *IEEE Transactions on Microwave Theory Technology*, **54**, 216–225.
[34] Harrington, R. F., 1961, *Time-Harmonic Electromagnetic Fields* (New York: McGraw-Hill).
[35] Avdeev, D. B., Kuvshinov, A. V., Pankratov, O. V. and Newman, G. A., 1997, High-performance three-dimensional electromagnetic modeling using modified Neumann series. Wide-band numerical solution and examples. *Journal of Geomagnetion and Geoelectricity*, **49**, 1519–1539.
[36] Pankratov, O. V., Avdeev, D. B. and Kuvshinov, A. V., 1995, Electromagnetic field scattering in a heterogeneous earth: A solution to the forward problem. *Physic of Solid Earth*, **31**, 201–209.
[37] Singer, B. S. and Fainberg, E. B., 1995, Generalization of iterative dissipative method for modeling electromagnetic fields in nonuniform media displacement currents. *Journal of Applied Geophysics*, **34**, 41–46.